ACS APPLIED MATERIALS & INTERFACES

Research Article

Cite This: ACS Appl. Mater. Interfaces XXXX, XXX, XXX−XXX

www.acsami.org

Metal−Organic Framework Thin Films on High-Curvature Nanostructures Toward Tandem Electrocatalysis

Phil De Luna,[†] Weibin Liang,[‡] Arijit Mallick,[‡] Osama Shekhah,[‡] F. Pelayo García de Arquer,[§] Andrew H. Proppe,[§] Petar Todorović,[§] Shana O. Kelley,[∥,⊥,#] Edward H. Sargent,*[,§] and Mohamed Eddaoudi*[,‡]

[†]Department of Materials Science and Engineering, University of Toronto, 184 College Street, Toronto, Ontario M5S 3E4, Canada

[‡]Division of Physical Science and Engineering (PSE), Advanced Membranes and Porous Materials Center (AMPM), Functional Materials Design, Discovery and Development (FMD[3]), King Abdullah University of Science and Technology (KAUST), Thuwal 23955-6900, Kingdom of Saudi Arabia

[§]Department of Electrical and Computer Engineering, University of Toronto, 35 St George Street, Toronto, Ontario M5S 1A4, Canada

[∥]Department of Biochemistry, Faculty of Medicine, [⊥]Department of Chemistry, Faculty of Arts and Science, and [#]Department of Pharmaceutical Sciences, Leslie Dan Faculty of Pharmacy, University of Toronto, Toronto, Ontario M5S 3M2, Canada

Supporting Information

ABSTRACT: In tandem catalysis, two distinct catalytic materials are interfaced to feed the product of one reaction into the next one. This approach, analogous to enzyme cascades, can potentially be used to upgrade small molecules such as CO_2 to more valuable hydrocarbons. Here, we investigate the materials chemistry of metal−organic framework (MOF) thin films grown on gold nanostructured microelectrodes (AuNMEs), focusing on the key materials chemistry challenges necessary to enable the applications of these MOF/AuNME composites in tandem catalysis. We applied two growth methods—layer-by-layer and solvothermal—to grow a variety of MOF thin films on AuNMEs and then characterized them using scanning electron microscopy, X-ray diffraction, and X-ray photoelectron spectroscopy. The MOF@AuNME materials were then evaluated for electrocatalytic CO_2 reduction. The morphology and crystallinity of the MOF thin films were examined, and it was found that MOF thin films were capable of dramatically suppressing CO production on AuNMEs and producing further-reduced carbon products such as CH_4 and C_2H_4. This work illustrates the use of MOF thin films to tune the activity of an underlying CO_2RR catalyst to produce further-reduced products.

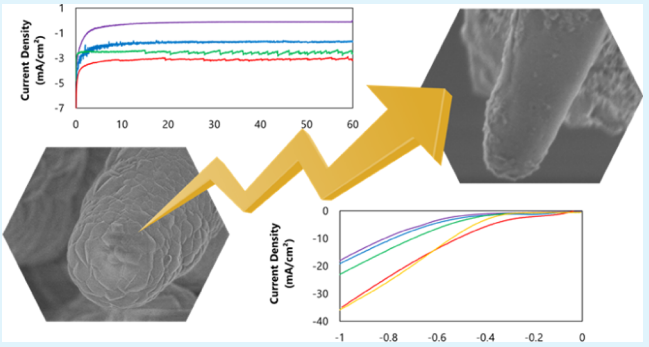

KEYWORDS: *metal−organic frameworks, thin films, electrocatalysis, tandem catalysis, high-curvature nanostructures, CO_2 reduction reaction*

INTRODUCTION

The past two decades have seen impressive advances in metal−organic frameworks (MOFs)—crystalline porous materials that are constructed via the assembly of metal ions or metal clusters and polytopic organic ligands. MOFs have attracted attention as a result of their modular nature, designed topology, high surface area, and chemical tunability.[1,2]

The hybrid organic−inorganic nature of MOFs permits reticular chemistry: predesigned molecular building blocks (MBBs) that possess designed-in chemical function, connectivity and geometry, enable a wide range of MOFs with prescribed topologies, pore systems, and chemical binding affinities.[3] Additionally, many types of MOFs can also be further functionalized using postsynthetic methods and by incorporation of other functions using a host−guest approach.[4] Conductive MOFs have also been recently developed whereby charge is propagated through the metal SBU units.[5] The versatile properties of MOFs enable their application in gas storage, separation, catalysis, sensing, and light harvesting.[6−8]

Sensor devices and membranes employing MOFs depend on the fabrication and deployment of these porous materials as thin films.[9−11] There exist several techniques for the deposition of MOF thin films including the direct growth from precursor solutions, the self-assembly of precursors, and layer-by-layer growth (also known as liquid-phase epitaxy) onto desired substrates.[9,12]

Received: March 25, 2018
Accepted: August 15, 2018
Published: August 21, 2018

DOI: 10.1021/acsami.8b04848
ACS Appl. Mater. Interfaces XXXX, XXX, XXX−XXX

High-curvature gold nanostructured microelectrodes (AuNMEs) are a new class of materials for electrochemical biosensing and electrocatalysis. These have been shown to increase probe display for DNA biosensing applications, leading to highly sensitive detection of biomolecules using electrochemical readout.[13] AuNMEs have been deployed in the detection of cancer biomarkers,[14] infectious pathogens,[15] and in organ transplant assessment.[16]

More recently, AuNMEs have been exploited in the electrochemical CO_2 reduction reaction (CO_2RR) for renewable fuel production.[17−22] AuNMEs were found to provide field-induced reagent concentration (FIRC),[20] where high local electric fields at the sharp tips concentrate positively charged cations that help stabilize CO_2RR intermediates. This led to an accelerated rate of CO_2RR, affording a record high current density (22 mA/cm^2) at low overpotential (0.24 V) with near unity selectivity [Faradaic efficiencies (FE) = 94%] for CO production.[17]

The benefits of FIRC can be extended by using AuNMEs as a support to grow/deposit thin layers of other catalysts. AuNMEs coated with a thin layer of tin sulfide were reduced under CO_2RR conditions to yield a catalyst that provided a high number of under-coordinated tin sites and thus achieved efficient formate production.[21] This system showed stability of over 40 h of operation with a current density of 55 mA/cm^2 and a FE of 93%. Additionally, this system has been explored by studying copper enrichment on the AuNMEs for tunable syngas production.[19] Overall, nanostructured electrodes displaying high-curvature morphologies can increase electrochemical activity and are thus of interest in synthetic fuel synthesis.

MOFs have seen intensified interest recently for CO_2RR, both electrochemically and photochemically.[23−28] Recent advances have focused on the use of MOFs deposited on inert substrates such as carbon paper.[29] Pioneering recent reports have begun to explore the combination of MOFs with highly active catalytic materials: a Re_3-MOF coated on silver nanocubes achieved plasmon-enhanced photocatalytic CO_2RR to CO.[23,30] In this work, the Ag nanocubes provided plasmon enhancement under visible light that led to an enhancement in photocatalytic activity on Re active centers covalently attached in the MOF pore.

MOFs combined with electrocatalysts offer promise in tandem catalysis, where the product at one catalytic center becomes the reactant at another catalytic center, analogous to biological enzyme cascades. One target for tandem catalysis is the reduction of CO_2 at the surface of a first catalyst CO; followed by ensuing reaction within the pores of a MOFs (proximate to the MOF/catalyst interface) to generate further-reduced higher-value products. To advance this goal, first step is the development of the materials chemistry to form of MOF thin films on nanostructured electrodes. In this development, the investigation of the electrochemical stability of the resultant materials is of particular importance and merits a focused study. A challenge of particular interest will be to develop MOF/electrocatalyst hybrids that reduce CO_2 to products of greater value than CO.

Here, we investigate the growth of MOF thin films on AuNMEs. We employ two different growth methods: the layer-by-layer method and the in situ solvothermal method. We find that these approaches each coat AuNMEs with MOF thin films and retain the underlying AuNME morphology. We study, using electrochemistry, electron microscopy, and X-ray photoelectron spectroscopy (XPS), the morphology and stability of these MOF thin films. We probe their CO_2RR activities and ascertain that MOF thin films are capable of completely suppressing CO production and that they produce detectable quantities of the reduced products CH_4 and C_2H_4.

RESULTS AND DISCUSSION

Design and Synthesis of MOF Thin Films on AuNMEs.

For the synthesis of MOF thin films on AuNMEs, we primarily focus on four well-studied stable MOFs: ZIF-8, Cu(bdc)·xH$_2$O, RE-ndc-**fcu**-MOF ndc = 1,4-naphthalenedicarboxylic acid, and Al-TCPP (TCPP = tetrakis(4-carboxyphenyl)-porphyrin).

ZIF-8 ($Zn(MeIM)_2$, MeIM = 2-methylimidazole) was selected for its high chemical and thermal stability (>500 °C) and large pore size (11.6 Å).[31,32] ZIF-8 has been explored for a range of catalytic applications,[33,34] including CO oxidation with embedded gold nanoparticles.[35]

Cu(bdc)·xH$_2$O contains open metal sites that are coordinated to water molecules, which may act as catalytic active sites.[32] This MOF has been investigated for CO_2 capture and was found to be particularly active when present as 2D nanosheets.[36]

Tunable rare-earth **fcu** MOFs (Re-**fcu**-MOF) are a class of MOFs composed of $[RE_6(\mu_3\text{-}OH)_8(O_2C-)_{12}]$ hexanuclear MBBs (MBB = molecular building block) bridged by a ditopic ligand, where the carbon atoms of the coordinated carboxylates act as points of extension. This RE-**fcu**-MOF is highly thermally stable up to 500 °C and chemically stable in water, acidic, and basic conditions.[34] The **fcu**-MOF platform has been explored mostly for its molecular sieving capabilities and hydrocarbon separations and has not previously been investigated for electrocatalysis.[37,38]

$Al_2(OH)_2$TCPP has porphyrin molecular units and was shown to be hydrolytically stable and thermally stable up to 400 °C.[35] Furthermore, it was found to be electrocatalytically active in CO_2RR for the production of CO.[39]

To fabricate MOF thin films on AuNMEs, we utilized two distinct thin-film growth approaches: layer-by-layer (or liquid phase epitaxy) and solvothermal methods (Figure 1). ZIF-8

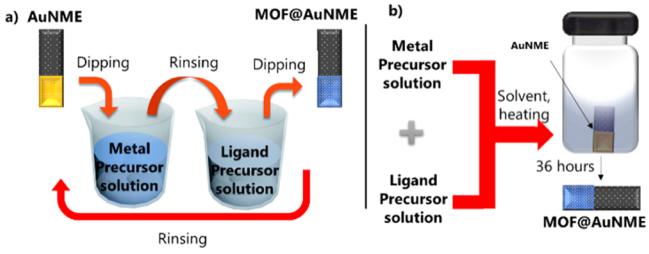

Figure 1. Schematic illustration of MOF thin film growth on AuNMEs by either the (a) layer-by-layer method or the (b) solvothermal method.

and Cu(bdc)·xH$_2$O were fabricated using the layer-by-layer method, whereas the RE-ndc-**fcu**-MOF and $Al_2(OH)_2$TCPP MOF were fabricated via the solvothermal method. In the layer-by-layer method, the AuNME substrate was first functionalized by an OH-terminated self-assembled monolayer (SAM).[40] Next, the surface-functionalized AuNME was immersed in the metal-containing precursor, rinsed with solvent, and then dipped in the organic ligand precursor, and repeated to the desired film thickness. In the solvothermal

DOI: 10.1021/acsami.8b04848
ACS Appl. Mater. Interfaces XXXX, XXX, XXX−XXX

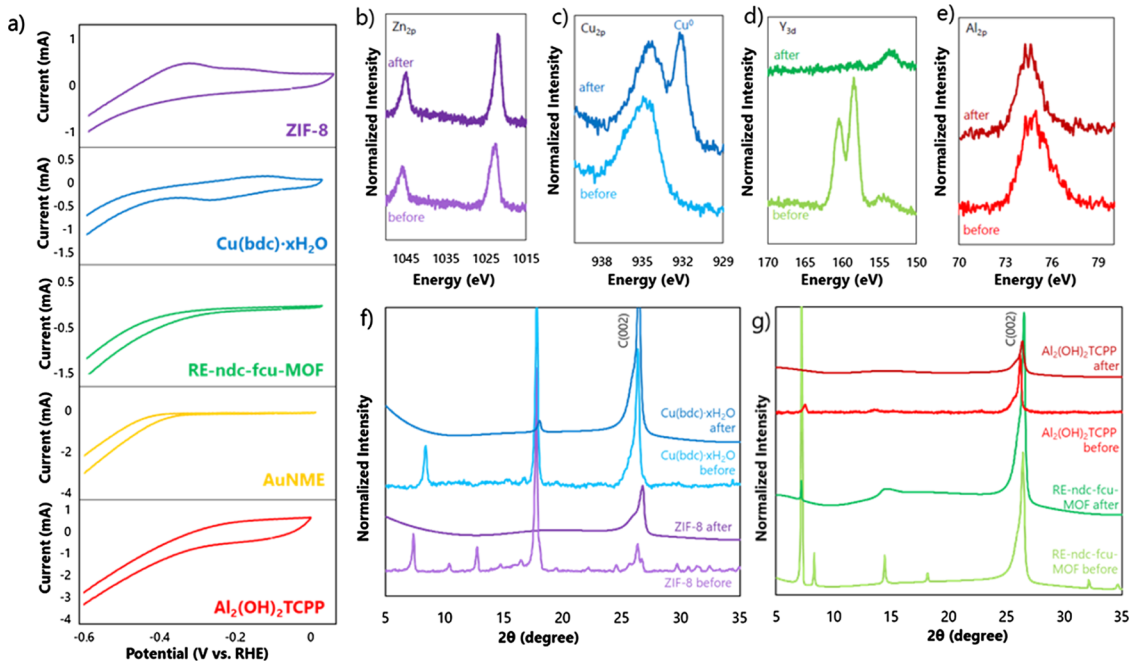

Figure 2. (a) CV (0 to −1 V vs RHE, 0.1 M $KHCO_3$) plots of the different thin-film MOFs deposited on Au NME. XPS measurements of Zn_{2p} (b), Cu_{2p} (c), Y_{3d} (d), and Al_{2p} (e) of AuNME/MOF thin films before and after reaction. XRD measurements of ZIF-8, Cu(bdc)·$x$$H_2O$ (f), RE-ndc-**fcu**-MOF, and $Al_2(OH)_2TCPP$ (g) thin films before and after reaction.

method, AuNME substrates were first functionalized using an OH-terminated SAM; then, the functionalized surface was immersed in a solution containing the metal precursor, the ligand precursor, and solvent; and the mixture was then heated at a fixed temperature for a specified time. Full synthesis details are available in the Experimental Section.

Characterization and Electrochemical Stability of MOF@AuNMEs. To study the electrochemical stability of the resultant thin-film MOFs on AuNMEs, we performed cyclic voltammetry (CV) experiments in the range of 0 V versus reversible hydrogen electrode (RHE) to −1 V versus RHE in CO_2 saturated 0.1 M $KHCO_3$ electrolyte (Figure 2a). The CV range with an upper limit of −1 V versus RHE was chosen to minimize irreversible reduction of the MOF.

For each MOF, the CV plots were found to be stable after 3 scans. ZIF-8, Cu(bdc)·$x$$H_2O$, and $Al_2(OH)_2TCPP$ exhibited reduction peaks that differed notably from that of the AuNME control. All MOFs showed similar reduction onset potentials of ∼−0.35 V versus RHE for either HER or CO_2RR.

Interestingly, the RE-ndc-**fcu**-MOF showed a CV curve similar to the AuNME control with no characteristic oxidation or reduction peak features as observed for the other evaluated MOFs. This suggests that RE-ndc-**fcu**-MOF is not electrochemically active or that the RE-ndc-**fcu**-MOF degraded immediately. To determine the chemical composition and the associated crystal structure after CO_2RR, we performed XPS and X-ray diffraction (XRD) experiments on the AuNME/MOF composites. CO_2RR was performed in a three-electrode H-cell setup with CO_2 saturated 0.1 M $KHCO_3$ as the electrolyte, platinum as the counter-electrode, and Ag/AgCl as the reference electrode. An applied potential of −0.5 V versus RHE was applied unless otherwise stated and sustained for over an hour of reaction. XPS results (Figure 2b–e) confirm the presence of Zn, Cu, and Al on the surface of the AuNME after reaction, indicating that the metal component of the MOF remains.

To assess the alteration/decrease of the MOF metal content after versus before reaction, XPS studies were performed to calculate the metal atomic percent. It was found that ZIF-8 was most stable, with only a 2.3% decrease of Zn; $Al_2(OH)_2TCPP$ exhibited a 12% decrease of Al, Cu(bdc)·$x$$H_2O$ showed a 32% decrease of Cu, and RE-ndc-**fcu**-MOF had the greatest amount with a 71% decrease of Y. These results suggest very little Y remaining after the reaction (Figure 2d), suggesting that the Y metal has leached into the electrolyte solution. This agrees with the CV experiments that show that RE-ndc-**fcu**-MOF exhibits a CV curve similar to AuNME. A peak around 932 eV (indicative of Cu^0) appeared in the Cu_{2p} spectrum after reaction (Figure 2c), suggesting that some of the copper within Cu(bdc)·$x$$H_2O$ was reduced during reaction. Both the Zn and Al spectra (Figure 2b,e) showed no immediate change, suggesting that ZIF-8 and $Al_2(OH)_2TCPP$ are more electrochemically stable than Cu(bdc)·$x$$H_2O$ and RE-ndc-**fcu**-MOF. XRD measurements show the clear change in the crystal structure for various MOF thin films before and after reaction. All XRD patterns showed characteristic peaks of the (002) planes at 26° from the carbon paper substrate. All MOF thin films show representative peaks corresponding to the respective MOF materials (Figure S2). For Cu(bdc)·$x$$H_2O$, there is a prominent peak at 8.4° and 17.8° which is indicative of the (001) and (002) planes, respectively,[41] but after reaction, this peak diminishes and a peak at 18.1° appears which is originated from the formation of a different material. ZIF-8 shows a peak around 7.5°, 10.1°, and 12.5° before reaction that corresponds to the (110), (200), and (211) planes,[32] but these peaks disappear after reaction suggesting a loss in crystallinity. The XRD pattern of $Al_2(OH)_2TCPP$ shows a peak at 7.5° before reaction, but no discernible peaks remaining after CO_2RR reaction. Interestingly, RE-ndc-**fcu**-MOF shows a highly crystalline structure with strong peaks at 7.2° and 8.3° corresponding to the (111) and (200) planes, respectively. After reaction, the crystallinity is severely

DOI: 10.1021/acsami.8b04848
ACS Appl. Mater. Interfaces XXXX, XXX, XXX−XXX

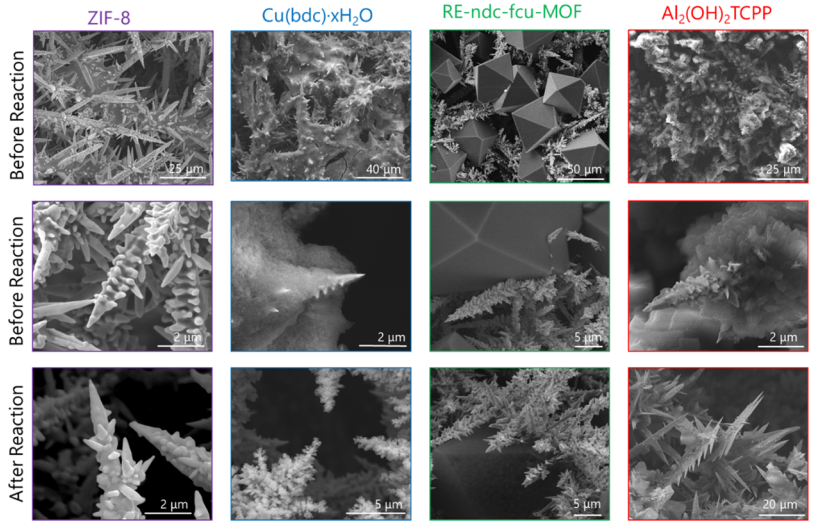

Figure 3. SEM images of ZIF-8, Cu(bdc)·xH$_2$O, RE-ndc-**fcu**-MOF, and Al$_2$(OH)$_2$TCPP thin films on AuNME before (top two rows) and after electrochemical reaction (bottom row).

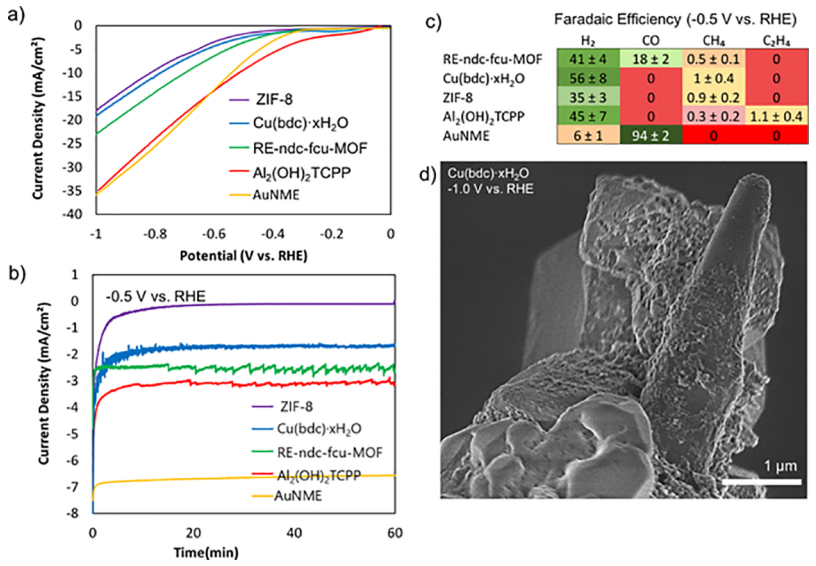

Figure 4. (a) LSV scans (0 to −1 V vs RHE, 0.1 M KHCO$_3$) of different MOF@AuNMEs and AuNME control. (b) Chronoamperometry plot (−0.5 V vs RHE, 0.1 M KHCO$_3$) of MOF@AuNMEs and AuNME control for an hour at −0.5 V vs RHE. (c) FEs of MOF@AuNMEs and AuNME control. (d) SEM image of the AuNME tip showing the underlying metal exposed after running at −1.0 V vs RHE.

diminished with only a weak peak at 7.2° remaining. These results suggest that CO$_2$RR conditions change/destroy the crystal structure of the deposited MOF thin film.

Scanning electron microscopy (SEM) images reveal the morphology of the MOF thin films before and after CO$_2$RR reaction (Figure 3). There are distinct differences between all structures and preparation methods, that is, layer-by-layer versus solvothermal. The layer-by-layer deposited ZIF-8 thin film coated the Au nanoneedles uniformly, with the nanostructured morphology remaining, which shows the power of the layer-by layer method.[31,41] The contrast in the SEM images before reaction suggests that the MOF thin film is thicker at the base of the needles rather than the tips (Figure 3). After reaction, the morphology of the MOF thin film was minimally changed, but the contrast between the base and tips of the nanoneedles was decreased, suggesting a degradation of the MOF. The Cu(bdc)·xH$_2$O morphology enveloped the Au nanoneedle structure and encased the needles, rather than uniformly coating them. The tips show a MOF thin film having a porous morphology before reaction; after reaction, the thin-film MOF morphology has condensed and formed dendritic crystal structures atop the nanoneedles. After reaction, the crystal structure of the MOF thin film again condensed, but this time rather than forming dendritic shapes such as with Cu(bdc)·xH$_2$O, Al$_2$(OH)$_2$TCPP showed thin flake-like structures. This suggests that the structure lost porosity and the final compressed structure shows an interesting correlation with the morphology before reaction, where porous MOF thin film make dendrites, whereas sheet thin films make large flake-like structures.

The solvothermal-deposited RE-ndc-**fcu**-MOF thin films formed octahedral crystals of approximately 50 μM in size rather than uniformly coating the AuNMEs. The RE-ndc-**fcu**-MOF crystals envelop the AuNME nanoneedles, and some gold nanoneedles can be seen protruding from the sides and edges of the RE-ndc-**fcu**-MOF crystal. The maintained high

DOI: 10.1021/acsami.8b04848
ACS Appl. Mater. Interfaces XXXX, XXX, XXX−XXX

crystallinity is reflected in the associated XRD pattern with many sharp peaks. For $Al_2(OH)_2TCPP$, the thin films show a morphology similar to $Cu(bdc)\cdot xH_2O$ with the thin film coating the AuNMEs and covering up their underlying nanoneedle morphology. A high-magnification SEM image shows that the thin-film MOFs are made up of aggregation of sheet-like crystals of $Cu(bdc)\cdot xH_2O$.

Electrocatalytic Activity of MOF@AuNMEs. To investigate the electrocatalytic activity of MOFs thin film on AuNMEs, we carried out CO_2RR for 1 h and examined CO_2RR activities after at least 1 h of reaction. Linear sweep voltammetry (LSV) scans on all MOF thin films on AuNMEs and on an AuNME control were performed to assess their catalytic onset potentials (Figure 4a). The potential range was chosen to be from 0 V versus RHE to −1 V versus RHE to avoid the electrochemical decomposition of the organic linkers within the MOFs.

Overall, the catalytic activity of MOF@AuNMEs lays below that of the native AuNME. Because MOFs typically have a modest electrical conductivity, they produce a lower rate of charge transfer to the catalytic active sites compared to the native AuNME. MOFs block a portion of CO-2RR active sites on the gold AuNME, decreasing CO production. Additionally, the porous confined structure of the MOF may retard the diffusion of both reactants and products.

The current densities at −1.0 V versus RHE ranged from 20 mA/cm^2 (for ZIF-8, $Cu(bdc)\cdot xH_2O$, and RE-ndc-**fcu**-MOF) to 35 mA/cm^2 ($Al_2(OH)_2TCPP$). Interestingly, the only MOF that displayed a LSV curve similar to the AuNME control was $Al_2(OH)_2TCPP$ suggesting good conductivity within the MOF@AuNME sample. The current densities at −0.5 V versus RHE show an initial decrease in the current density followed by a stable and sustained operation for up to 1 h (Figure 4b). ZIF-8 showed almost no activity with a stable current density of −0.1 mA/cm^2, whereas $Cu(bdc)\cdot xH_2O$ was slightly higher with −1.7 mA/cm^2. RE-ndc-**fcu**-MOF showed a current density of −2.5 mA/cm^2, and $Al_2(OH)_2TCPP$ exhibited a current density of −3.1 mA/cm^2. The noise that appears in the RE-ndc-**fcu**-MOF around 16 min of operation is indicative of bubble generation: gas bubble evolution accelerated at this time due to a change in the stir rate. The trends in current density remain consistent with the LSV curves.

The gaseous products were then determined using gas chromatography, and the FE were calculated (Figure 4c). NMR analysis of the electrolyte after reaction showed no trace of liquid products. It was found that all MOF thin films produced mostly hydrogen with FEs for HER from 35 ± 3% (ZIF-8) to 56 ± 8% ($Cu(bdc)\cdot xH_2O$). All MOFs showed trace amounts of methane (CH_4) at <1% FE and $Al_2(OH)_2TCPP$ even showed an ethylene (C_2H_4) FE of 1.1 ± 0.4%. The only MOF that exhibited CO production, the main product for the AuNME substrate, was RE-ndc-**fcu**-MOF with a FE of 18 ± 2%. The MOFs that completely covered the AuNME either by conformally coating or by enveloping the morphologies showed no CO production. As RE-ndc-**fcu**-MOF crystals grew on the AuNME in segregated particles, there were still many exposed AuNME active sites that could contribute to CO production, explaining the 18% FE for thin-film RE-ndc-**fcu**-MOF on AuNME.

To test whether the CO production was attributed only to the underlying AuNMEs, we sought a way to remove partially the MOF thin film from the AuNME. Thus, we ran the CO_2RR at a more negative potential of −1.0 V versus RHE in hopes of electrochemically reducing a portion of the MOF. At −1.0 V versus RHE, the CO FE of $Cu(bdc)\cdot xH_2O$ was 15.7 ± 3%, an increase from no CO production at −0.5 V versus RHE. SEM images reveal that $Cu(bdc)\cdot xH_2O$ was selectively removed only from the tips of the AuNME (Figure 4d). This suggests that the activity of the AuNME is located at the tips, which is a direct experimental evidence for the proposed FIRC phenomenon as previously reported.[17,18] All MOFs that uniformly coated the AuNMEs were able to fully suppress the CO production from AuNMEs, attesting to the coverage quality of the MOF thin films deposited via layer-by-layer and solvothermal methods. Although the majority of the current went toward HER, all MOFs produced detectable amounts of CO_2RR products. If these products came from the degradation of the MOF itself, one would expect an additional set of diverse carbon species in the NMR spectra, but no further products were found in NMR. This suggests that the MOFs@AuNME was capable of producing CO_2RR products CH_4 and C_2H_4 that are further reduced from CO. Of note was the C_2H_4 production with $Al_2(OH)_2TCPP$. This production is most likely from reaction of CO_2 with the porphyrin linker. Previous reports on a copper−porphyrin complex deposited on carbon paper also showed CH_4 and C_2H_4 as minor CO_2RR products.[42] Ethylene production has been shown to rely heavily on CO coverage and occur via CO dimerization.[43] Ideally, high local CO generation at the surface of AuNME could promote C_2H_4 formation at a proximate MOF active site. This suggests one explanation for why CH_4 and C_2H_4 were observed in the case of the porphyrin-containing $Al_2(OH_2)TCPP$.

While the promise of tandem catalysis, where CO_2 is converted on the surface of gold to one product and then in turn may be converted in the pores of a MOF, is attractive, there remain areas of improvement that we list below:

1. The electrical conductivity of the MOF.
2. The electrochemical stability of the MOF at reducing potentials.
3. The catalytic activity of the MOF.
4. Uniform coating of MOFs to retain underlying nanostructure.
5. Sufficient pore size capable of adsorbing/concentrating CO_2 and afford product diffusion to and from the metal/MOF interface.

An effective MOF for tandem applications should be sufficiently conductive to carry charge from the underlying metal substrate to the active sites within the MOF pores, be catalytically active for CO_2RR, be highly stable and not susceptible to electrochemical reduction or change under applied bias and have large enough pores to facilitate product and reactant kinetics. Solutions to these challenge areas include using nonaqueous solvent, cocatalysts, and flow-cell configurations that allow stable operation of CO_2RR at a three-phase interface.[44]

CONCLUSIONS

We report the synthesis of MOF thin films via two methods, layer-by-layer and solvothermal deposition, on gold nanostructured microrelectrodes and their subsequent investigation for electrocatalytic CO_2RR activity. We find that the layer-by-layer method produces the most uniformly coated MOF thin films because of the use of a SAM binder. The morphology

DOI: 10.1021/acsami.8b04848
ACS Appl. Mater. Interfaces XXXX, XXX, XXX−XXX

changes of the MOF thin films before and after reaction suggest that their porosity and crystal structures are highly susceptible to change under a negative applied bias and in CO_2 saturated 0.1 M $KHCO_3$ electrolyte. XRD and XPS studies further revealed that whereas the metal ions of the MOFs remained for the majority of MOFs, the crystal structures were either distorted or severely disrupted. The major MOF@AuNME product was hydrogen, but well-coated MOF thin films were found to completely suppress CO and produce small amounts of CH_4 and C_2H_4. Interestingly, their coating and suppression of CO production from AuNME could be reversed by applying a sufficiently high negative applied potential. At −1.0 V versus RHE, the tips of the AuNMEs become exposed because of MOF degradation and CO production may occur. We provide five synergistic pathways for improvement of thin-film MOFs on nanostructured metal catalysts to realize tandem catalysis. This work represents the first report of MOF thin films being utilized to tune the CO_2RR activities of an underlying catalyst.

EXPERIMENTAL SECTION

Synthesis and Characterization of MOF Thin Films on AuNMEs. The Cu (bdc)·$x$$H_2O$ MOF was grown on a prefunctionalized AuNME substrate with the of 16 mercaptohexadecanoic acid SAM by the layer-by-layer method.[45,46] The AuNME substrate was then mounted on the Teflon sample holder in the robot vertically using Teflon screws. (1) The substrate was immersed in 1 mM of $Cu_2(CH_3COO)_4^{\bullet}$ ethanol solution for 3 min solution for 90 s, (2) washed with the fresh solvent, (3) immersion in 0.1 mM of benzene dicarboxylic acid (bdc) ethanolic solution for 5 min at room temperature, and (4) washed with the fresh solvent. This process was considered to be as one cycle and then repeated for 150 times, in order to grow more layers (see Figure 1a). After 150 cycles, the AuNME substrate was allowed to dry slowly in ambient air overnight.

ZIF-8 thin films were grown on a prefunctionalized AuNME substrate with the 11-mercaptoundecanol (MUD) SAM by the layer-by-layer method similar to the Cu (bdc)·$x$$H_2O$ MOF. The AuNME substrate was then mounted on the Teflon sample holder in the robot vertically using Teflon screws. The growth was performed briefly using the following steps: (1) the substrate was immersed in a 2 mM of $Zn(NO_3)_2$·$6H_2O$ methanol solution for 3 min, (2) washed with the fresh solvent, (3) immersion in 2 mM of 2-methylimidazole methanol solution for 5 min, and (4) washed with the fresh solvent. This process was considered to be as one cycle and then repeated 200 times, in order to grow more layers (see Figure 1a). After 200 cycles, the AuNME substrate was allowed to dry slowly in ambient air overnight.

Thin films of the RE-ndc-**fcu**-MOF were prepared using a solvothermal approach through heating a solution that containing $Y(NO_3)_3$·$6H_2O$ (0.087 mmol), 1,4-naphthalene dicarboxylic acid (0.087 mmol), 2-fluorobenzoic acid (0.70 mmol) dimethylformamide (DMF) (6.0 mL), deionized H_2O (1 mL), and nitric acid (0.4 mL of 4 M solution in DMF), all combined in a 20 mL scintillation vial. A prefunctionalized AuNME substrate with MUD SAM, which was placed inside the vial, which was sealed and heated to 115 °C for 48 h. The AuNME substrate was removed and rinsed with DMF and then immersed in ethanol for 3 days, during which the ethanol solution was refreshed three times daily.

Thin films of Al−TCPP were grown using a solvothermal approach through heating a solution that contains TCPP (0.126 mmol), $AlCl_3$·$6H_2O$ (0.25 mmol), DMF (5 mL), and deionized H_2O (5 mL) in a 23 mL autoclave. We chose to use DMF as a solvent to improve the solubility of the linker molecule, which allows us to work at a lower reaction temperature of 150 °C, a prefunctionalized Au needle with the MUD SAM was placed inside the vial and sealed and heated to 150 °C for 36 h and then cooled to room temperature. The Au needle substrates were collected and washed with about 10 mL of anhydrous DMF and immersed in 10 mL of ethanol for 3 days, during which time the ethanol was replaced three times per day.

XRD measurements were carried out at room temperature on a PANalytical X'Pert Pro diffractometer 45 kV, 40 mA for Cu Kα (λ = 1.5418 Å), with a scan rate of 1.0° min^{-1} and a step size of 0.01° in 2θ. SEM characterization was performed using an FEI Quanta 600 field emission SEM (accelerating voltage: 30 kV).

ASSOCIATED CONTENT

Supporting Information

The Supporting Information is available free of charge on the ACS Publications website at DOI: 10.1021/acsami.8b04848.

Detailed materials and methods, MOF thin-film synthesis, and additional electrochemical characterization (PDF)

AUTHOR INFORMATION

Corresponding Authors

*E-mail: ted.sargent@utoronto.ca (E.H.S.).
*E-mail: mohamed.eddaoudi@kaust.edu.sa (M.E.).

ORCID

Phil De Luna: 0000-0002-7729-8816
Osama Shekhah: 0000-0003-1861-9226
Shana O. Kelley: 0000-0003-3360-5359
Edward H. Sargent: 0000-0003-0396-6495
Mohamed Eddaoudi: 0000-0003-1916-9837

Author Contributions

All authors have given approval to the final version of the manuscript. P.D.L. performed electrochemical experiments and SEM measurements. W.L., A.M., and O.S. fabricated the MOF thin films. A.H.P. performed XPS measurements. P.T. performed XRD measurements. O.S. and P.D.L. wrote the manuscript. E.H.S. and M.E. designed and supervised the study.

Notes

The authors declare no competing financial interest.

ACKNOWLEDGMENTS

This publication is based in part on work supported by the Center Partnership Funds Program, made by King Abdullah University of Science and Technology (KAUST), by the Ontario Research Fund Research Excellence Program, and by the Natural Sciences and Engineering Research Council (NSERC) of Canada. P.D.L. wishes to thank the Natural Sciences and Engineering Research Council (NSERC) of Canada for support in the form of the Canadian Graduate Scholarship—Doctoral award.

ABBREVIATIONS

MOF, metal−organic frameworks; SEM, scanning electron microscopy; XRD, X-ray diffraction; XPSX-ray photoelectron spectroscopyCO_2RR, X-ray photoelectron spectroscopy-CO_2RRcarbon dioxide reduction reaction; AuNME, gold nanostructured microelectrodes; MBBs, molecular building blocks; FIRCfield-induced reagent concentrationLSV, field-induced reagent concentrationLSVlinear sweep voltammetry; NMR, nuclear magnetic resonance

REFERENCES

(1) Zhou, H.-C.; Long, J. R.; Yaghi, O. M. Introduction to Metal-Organic Frameworks. *Chem. Rev.* **2012**, *112*, 673−674.

DOI: 10.1021/acsami.8b04848
ACS Appl. Mater. Interfaces XXXX, XXX, XXX−XXX

(2) Kuppler, R. J.; Timmons, D. J.; Fang, Q.-R.; Li, J.-R.; Makal, T. A.; Young, M. D.; Yuan, D.; Zhao, D.; Zhuang, W.; Zhou, H.-C. Potential Applications of Metal-Organic Frameworks. *Coord. Chem. Rev.* **2009**, *253*, 3042−3066.
(3) Guillerm, V.; Kim, D.; Eubank, J. F.; Luebke, R.; Liu, X.; Adil, K.; Lah, M. S.; Eddaoudi, M. A supermolecular building approach for the design and construction of metal-organic frameworks. *Chem. Soc. Rev.* **2014**, *43*, 6141−6172.
(4) Song, X.; Kim, T. K.; Kim, H.; Kim, D.; Jeong, S.; Moon, H. R.; Lah, M. S. Post-Synthetic Modifications of Framework Metal Ions in Isostructural Metal-Organic Frameworks: Core-Shell Heterostructures via Selective Transmetalations. *Chem. Mater.* **2012**, *24*, 3065−3073.
(5) Sheberla, D.; Bachman, J. C.; Elias, J. S.; Sun, C.-J.; Shao-Horn, Y.; Dincă, M. Conductive MOF Electrodes for Stable Supercapacitors with High Areal Capacitance. *Nat. Mater.* **2017**, *16*, 220−224.
(6) Furukawa, H.; Cordova, K. E.; O'Keeffe, M.; Yaghi, O. M. The Chemistry and Applications of Metal-Organic Frameworks. *Science* **2013**, *341*, 1230444.
(7) Wang, H.; Zhu, Q.-L.; Zou, R.; Xu, Q. Metal-Organic Frameworks for Energy Applications. *Chem* **2017**, *2*, 52−80.
(8) Pettinari, C.; Marchetti, F.; Mosca, N.; Tosi, G.; Drozdov, A. Application of Metal−Organic Frameworks. *Polymer International*; John Wiley & Sons, Ltd June 1, 2017; pp 731−744.
(9) Shekhah, O.; Liu, J.; Fischer, R. A.; Wöll, C. MOF Thin Films: Existing and Future Applications. *Chem. Soc. Rev.* **2011**, *40*, 1081.
(10) Campbell, M.; Dincă, M. Metal-Organic Frameworks as Active Materials in Electronic Sensor Devices. *Sensors* **2017**, *17*, 1108.
(11) Qiu, S.; Xue, M.; Zhu, G. Metal-organic framework membranes: from synthesis to separation application. *Chem. Soc. Rev.* **2014**, *43*, 6116−6140.
(12) Liu, J.; Shekhah, O.; Stammer, X.; Arslan, H. K.; Liu, B.; Schüpbach, B.; Terfort, A.; Wöll, C. Deposition of Metal-Organic Frameworks by Liquid-Phase Epitaxy: The Influence of Substrate Functional Group Density on Film Orientation. *Materials* **2012**, *5*, 1581−1592.
(13) De Luna, P.; Mahshid, S. S.; Das, J.; Luan, B.; Sargent, E. H.; Kelley, S. O.; Zhou, R. High-Curvature Nanostructuring Enhances Probe Display for Biomolecular Detection. *Nano Lett.* **2017**, *17*, 1289−1295.
(14) Fang, Z.; Soleymani, L.; Pampalakis, G.; Yoshimoto, M.; Squire, J. A.; Sargent, E. H.; Kelley, S. O. Direct Profiling of Cancer Biomarkers in Tumor Tissue Using a Multiplexed Nanostructured Microelectrode Integrated Circuit. *ACS Nano* **2009**, *3*, 3207−3213.
(15) Das, J.; Cederquist, K. B.; Zaragoza, A. A.; Lee, P. E.; Sargent, E. H.; Kelley, S. O. An Ultrasensitive Universal Detector Based on Neutralizer Displacement. *Nat. Chem.* **2012**, *4*, 642−648.
(16) Sage, A. T.; Besant, J. D.; Mahmoudian, L.; Poudineh, M.; Bai, X.; Zamel, R.; Hsin, M.; Sargent, E. H.; Cypel, M.; Liu, M.; Keshavjee, S.; Kelley, S. O. Fractal Circuit Sensors Enable Rapid Quantification of Biomarkers for Donor Lung Assessment for Transplantation. *Sci. Adv.* **2015**, *1*, No. e1500417.
(17) Liu, M.; Pang, Y.; Zhang, B.; De Luna, P.; Voznyy, O.; Xu, J.; Zheng, X.; Dinh, C. T.; Fan, F.; Cao, C.; de Arquer, F. P. G.; Safaei, T. S.; Mepham, A.; Klinkova, A.; Kumacheva, E.; Filleter, T.; Sinton, D.; Kelley, S. O.; Sargent, E. H. Enhanced Electrocatalytic CO2 Reduction via Field-Induced Reagent Concentration. *Nature* **2016**, *537*, 382−386.
(18) Klinkova, A.; De Luna, P.; Dinh, C.-T.; Voznyy, O.; Larin, E. M.; Kumacheva, E.; Sargent, E. H. Rational Design of Efficient Palladium Catalysts for Electroreduction of Carbon Dioxide to Formate. *ACS Catal.* **2016**, *6*, 8115−8120.
(19) Ross, M. B.; Dinh, C. T.; Li, Y.; Kim, D.; De Luna, P.; Sargent, E. H.; Yang, P. Tunable Cu Enrichment Enables Designer Syngas Electrosynthesis from CO2. *J. Am. Chem. Soc.* **2017**, *139*, 9359−9363.
(20) De Luna, P.; Quintero-Bermudez, R.; Dinh, C.-T.; Ross, M. B.; Bushuyev, O. S.; Todorović, P.; Regier, T.; Kelley, S. O.; Yang, P.; Sargent, E. H. Catalyst Electro-Redeposition Controls Morphology and Oxidation State for Selective Carbon Dioxide Reduction. *Nat. Catal.* **2018**, *1*, 103−110.
(21) Zheng, X.; De Luna, P.; de Arquer, F. P. G.; Zhang, B.; Becknell, N.; Ross, M. B.; Li, Y.; Banis, M. N.; Li, Y.; Liu, M.; Voznyy, O.; Dinh, C. T.; Zhuang, T.; Stadler, P.; Cui, Y.; Du, X.; Yang, P.; Sargent, E. H. Sulfur-Modulated Tin Sites Enable Highly Selective Electrochemical Reduction of CO 2 to Formate. *Joule* **2017**, *1*, 794−805.
(22) Zheng, X.; Zhang, B.; De Luna, P.; Liang, Y.; Comin, R.; Voznyy, O.; Han, L.; de Arquer, F. P. G.; Liu, M.; Dinh, C. T.; Regier, T.; Dynes, J. J.; He, S.; Xin, H. L.; Peng, H.; Prendergast, D.; Du, X.; Sargent, E. H. Theory-Driven Design of High-Valence Metal Sites for Water Oxidation Confirmed Using in Situ Soft X-Ray Absorption. *Nat. Chem.* **2017**, *10*, 149−154.
(23) Choi, K. M.; Kim, D.; Rungtaweevoranit, B.; Trickett, C. A.; Barmanbek, J. T. D.; Alshammari, A. S.; Yang, P.; Yaghi, O. M. Plasmon-Enhanced Photocatalytic CO2 Conversion within Metal-Organic Frameworks under Visible Light. *J. Am. Chem. Soc.* **2017**, *139*, 356−362.
(24) Chen, Y.; Wang, D.; Deng, X.; Li, Z. Metal-organic frameworks (MOFs) for photocatalytic CO2 reduction. *Catal. Sci. Technol.* **2017**, *7*, 4893−4904.
(25) Wang, D.; Huang, R.; Liu, W.; Sun, D.; Li, Z. Fe-Based MOFs for Photocatalytic CO2 Reduction: Role of Coordination Unsaturated Sites and Dual Excitation Pathways. *ACS Catal.* **2014**, *4*, 4254−4260.
(26) Diercks, C. S.; Liu, Y.; Cordova, K. E.; Yaghi, O. M. The Role of Reticular Chemistry in the Design of CO2 Reduction Catalysts. *Nat. Mater.* **2018**, *17*, 301−307.
(27) Wu, H. B.; Lou, X. W. D. Metal-Organic Frameworks and Their Derived Materials for Electrochemical Energy Storage and Conversion: Promises and Challenges. *Sci. Adv.* **2017**, *3*, No. eaap9252.
(28) Zhang, H.; Nai, J.; Yu, L.; Lou, X. W. D. Metal-Organic-Framework-Based Materials as Platforms for Renewable Energy and Environmental Applications. *Joule* **2017**, *1*, 77−107.
(29) Hod, I.; Sampson, M. D.; Deria, P.; Kubiak, C. P.; Farha, O. K.; Hupp, J. T. Fe-Porphyrin-Based Metal-Organic Framework Films as High-Surface Concentration, Heterogeneous Catalysts for Electrochemical Reduction of CO2. *ACS Catal.* **2015**, *5*, 6302−6309.
(30) Trickett, C. A.; Helal, A.; Al-Maythalony, B. A.; Yamani, Z. H.; Cordova, K. E.; Yaghi, O. M. The chemistry of metal-organic frameworks for CO2 capture, regeneration and conversion. *Nat. Rev. Mater.* **2017**, *2*, 17045.
(31) Shekhah, O.; Fu, L.; Sougrat, R.; Belmabkhout, Y.; Cairns, A. J.; Giannelis, E. P.; Eddaoudi, M. Successful Implementation of the Stepwise Layer-by-Layer Growth of MOF Thin Films on Confined Surfaces: Mesoporous Silica Foam as a First Case Study. *Chem. Commun.* **2012**, *48*, 11434.
(32) Shekhah, O.; Eddaoudi, M. The Liquid Phase Epitaxy Method for the Construction of Oriented ZIF-8 Thin Films with Controlled Growth on Functionalized Surfaces. *Chem. Commun.* **2013**, *49*, 10079.
(33) Miralda, C. M.; Macias, E. E.; Zhu, M.; Ratnasamy, P.; Carreon, M. A. Zeolitic Imidazole Framework-8 Catalysts in the Conversion of CO2 to Chloropropene Carbonate. *ACS Catal.* **2012**, *2*, 180−183.
(34) Yang, L.; Xie, C.; Li, Y.; Guo, L.; Nie, M.; Zhang, J.; Yan, Z.; Wang, J.; Wang, W. Polymerization of Alkylsilanes on ZIF-8 to Hierarchical Siloxane Microspheres and Microflowers. *Catalysts* **2017**, *7*, 77.
(35) Jiang, H.-L.; Liu, B.; Akita, T.; Haruta, M.; Sakurai, H.; Xu, Q. Au@ZIF-8: CO Oxidation over Gold Nanoparticles Deposited to Metal−Organic Framework. *J. Am. Chem. Soc.* **2009**, *131*, 11302−11303.
(36) Rodenas, T.; Luz, I.; Prieto, G.; Seoane, B.; Miro, H.; Corma, A.; Kapteijn, F.; Xamena, F. X. L. i.; Gascon, J. Metal-Organic Framework Nanosheets in Polymer Composite Materials for Gas Separation. *Nat. Mater.* **2015**, *14*, 48−55.
(37) Xue, D.-X.; Cairns, A. J.; Belmabkhout, Y.; Wojtas, L.; Liu, Y.; Alkordi, M. H.; Eddaoudi, M. Tunable Rare-Earth Fcu-MOFs: A Platform for Systematic Enhancement of CO2 Adsorption Energetics and Uptake. *J. Am. Chem. Soc.* **2013**, *135*, 7660−7667.
(38) Xue, D.-X.; Belmabkhout, Y.; Shekhah, O.; Jiang, H.; Adil, K.; Cairns, A. J.; Eddaoudi, M. Tunable Rare Earth Fcu-MOF Platform:

DOI: 10.1021/acsami.8b04848
ACS Appl. Mater. Interfaces XXXX, XXX, XXX−XXX

Access to Adsorption Kinetics Driven Gas/Vapor Separations via Pore Size Contraction. *J. Am. Chem. Soc.* **2015**, *137*, 5034−5040.
(39) Fateeva, A.; Chater, P. A.; Ireland, C. P.; Tahir, A. A.; Khimyak, Y. Z.; Wiper, P. V.; Darwent, J. R.; Rosseinsky, M. J. A Water-Stable Porphyrin-Based Metal-Organic Framework Active for Visible-Light Photocatalysis. *Angew. Chem., Int. Ed.* **2012**, *51*, 7440−7444.
(40) Shekhah, O. Layer-by-Layer Method for the Synthesis and Growth of Surface Mounted Metal-Organic Frameworks (SURMOFS). *Materials* **2010**, *3*, 1302−1315.
(41) Chernikova, V.; Shekhah, O.; Eddaoudi, M. Advanced Fabrication Method for the Preparation of MOF Thin Films: Liquid-Phase Epitaxy Approach Meets Spin Coating Method. *ACS Appl. Mater. Interfaces* **2016**, *8*, 20459−20464.
(42) Weng, Z.; Jiang, J.; Wu, Y.; Wu, Z.; Guo, X.; Materna, K. L.; Liu, W.; Batista, V. S.; Brudvig, G. W.; Wang, H. Electrochemical CO2 Reduction to Hydrocarbons on a Heterogeneous Molecular Cu Catalyst in Aqueous Solution. *J. Am. Chem. Soc.* **2016**, *138*, 8076−8079.
(43) Montoya, J. H.; Shi, C.; Chan, K.; Nørskov, J. K. Theoretical Insights into a CO Dimerization Mechanism in CO2 Electroreduction. *J. Phys. Chem. Lett.* **2015**, *6*, 2032−2037.
(44) Dinh, C.-T.; Burdyny, T.; Kibria, M. G.; Seifitokaldani, A.; Gabardo, C. M.; de Arquer, F. P. G.; Kiani, A.; Edwards, J. P.; De Luna, P.; Bushuyev, O. S.; Zou, C.; Quintero-Bermudez, R.; Pang, Y.; Sinton, D.; Sargent, E. H. CO2electroreduction to ethylene via hydroxide-mediated copper catalysis at an abrupt interface. *Science* **2018**, *360*, 783−787.
(45) Shekhah, O.; Arslan, H. K.; Chen, K.; Schmittel, M.; Maul, R.; Wenzel, W.; Wöll, C. Post-Synthetic Modification of Epitaxially Grown, Highly Oriented Functionalized MOF Thin Films. *Chem. Commun.* **2011**, *47*, 11210.
(46) Azzam, E. M. S.; Bashir, A.; Shekhah, O.; Alawady, A. R. E.; Birkner, A.; Grunwald, C.; Wöll, C. Fabrication of a Surface Plasmon Resonance Biosensor Based on Gold Nanoparticles Chemisorbed onto a 1,10-Decanedithiol Self-Assembled Monolayer. *Thin Solid Films* **2009**, *518*, 387−391.

DOI: 10.1021/acsami.8b04848
ACS Appl. Mater. Interfaces XXXX, XXX, XXX−XXX